A penalization technique applied to the "Volume-Of-Fluid" method: Wettability condition on immersed boundaries

Pierre Horgue [a,*], Marc Prat [a,b], Michel Quintard [a,b]

[a] Université de Toulouse, INPT, UPS, IMFT (Institut de Mécanique des Fluides de Toulouse), Allée Camille Soula, 31400 Toulouse, France
[b] CNRS, IMFT, 31400 Toulouse, France

A B S T R A C T

A penalization approach is presented to simulate two-phase flow in the presence of immersed solid boundaries so as to consider highly complex objects such as porous media microstructures. Based on the standard Volume-Of-Fluid formulation, the method takes into account the wettability effects which may occur on the surface of immersed solid boundaries. A spatial shift between the no-slip and the wettability conditions is introduced to make the method stable, regardless of the simulation parameters. The penalized VOF model and the numerical choices are then validated by a series of tests on capillary-dominated flows, which represent the most challenging cases for VOF simulations.

Keywords:
Penalization
Volume-Of-Fluid
Two-phase flow
Immersed boundary

1. Introduction

The modeling of two-phase flows in complex geometries is still a major challenge for two main reasons. On the one hand, existing multiphase flow methods developed to simulate the interfacial dynamics usually require significant computation time, especially methods with one-fluid formulation, such as the "Level-Set" [1], the "Cahn–Hilliard" [2] or the "Volume-Of-Fluid" (VOF) method [3]. The advantage of these methods lies in their ability to simulate *accurately* the various phenomena involved in multiphase flows, in contrast to explicit interface tracking methods for which some problems present a particular challenge, like, for example, bubble coalescence or snap-off. However, the large computation time required by these methods limits their use in terms of simulation domain size and partly explains their relatively recent development.

On the other hand, simulating flow in complex geometries constitutes generally an additional difficulty. In computational fluid dynamics, this can be handled by two main approaches: the use of unstructured meshes or immersed boundary methods. The immersed boundary methods offer an interesting alternative to usual methods, i.e., methods which operate on a geometry-conformal grid. Indeed, the representation of solid boundaries on Cartesian grids produces generally lower computational and memory costs as well as easier mesh generation. Constitutive equations must be modified by adding terms which take into account the fluid–structure interactions with the immersed boundaries [4,5]. Various immersed boundary methods have been developed to take into account the presence of obstacles such as level-set method [6], the ghost-fluid method [7] or the penalization method [4,5]. Readers interested in comprehensive reviews on the immersed boundary methods are referred to the papers by Peskin [8] or Mittal and Laccarino [9].

In this study, we develop a volume penalization approach applied to a tracking interface method, the VOF method, in order to simulate two-phase flow in the presence of wettability conditions on immersed solid boundaries. The penalization technique involves the introduction of a velocity penalization term in the momentum equation, normally applied at the surface of the immersed objects. Saiki and Birigen [10] showed the necessity to apply the penalization term on the volume of the immersed objects and not only on the immersed solid surface, in order to simulate accurately the flow at high Reynolds numbers. This volume penalization approach, which is used in this work, is based on the idea that the immersed solid object is a porous medium whose permeability tends to zero. The method has been used successfully to simulate incompressible viscous flows [11], turbulent flows [12], compressible flows [13], and, more recently, incompressible flows with scalar advection–diffusion [14]. Penalization techniques have also been used for modeling multiphase flows in complex geometries [15–17]. Prodanovic and Bryant [15] enforced "a no-penetration" constraint with a Level-Set method to prevent the invasion of the fluid into the solid domain. This constraint induces a fluid–fluid interface perfectly aligned with the solid surface, which in fact

* Corresponding author.
E-mail address: pierre.horgue@imft.fr (P. Horgue).

means a perfectly wetting condition on the immersed boundary (contact angle $\theta = 0°$). The penalty method with a "no-penetration" condition has been used in conjunction with the VOF method to simulate two-phase flows interacting with moving solids [16]. Recently, the penalized Level-Set method has been extended to simulate capillary-controlled displacements with non-zero contact angles [17]. The major goal of the work was to find equilibrium configurations, i.e., interfaces with constant curvature (if no gravity effects). To achieve such a goal, the method involves the introduction of an artificial fluid velocity in the (penalized) solid domain, in order to enforce the correct contact angle. The authors tested successfully their scheme on static situations (i.e., steady solutions or quasi-static displacements). The proposed scheme works in principle well with capillary dominant flows, but it may create inaccurate transient simulations when viscous forces are also at play. Another technique is based on the introduction of a wettability coefficient to simulate the contact line of a three phase system [18]. The penalization wettability coefficient modifies, close to the contact line, the "color" function which defines the interface position in order to impose contact angles between the three phases. In this method, a correlation between the coefficient ($\in [0; 1]$) and the contact angle ($\in [0 : 180°]$) needs to be defined numerically.

In this paper, we develop a penalized VOF method, without additional coefficient, to simulate multiphase flows in the presence of complex objects, focusing the study on the wettability condition applied on the immersed boundaries, and taking into account the potential impact of viscous forces on the interface dynamics. We first present the mathematical description of the model in Section 2, in particular the development of a penalized version of the constitutive equations of the VOF method. Then, the numerical implementation of the model using the OpenFOAM® platform is presented in Section 3, giving in details the discretization of the model equations. The developed code is based on the standard OpenFOAM® VOF model, but with the addition of some features recently proposed by Raeini et al. [19], such as smoothing operations improving the interface curvature computation (see Section 3.3), which may have significant effects for capillary-dominated flows. Section 4 describes the validation of the method, which is performed on several two-dimensional capillary-dominated flows by comparing numerical results with the results obtained with the usual VOF model. The three-dimensional simulation of a drop impact on a solid flat surface is also performed and qualitatively compared with experimental results.

2. Mathematical description

After a brief introduction to the VOF method, we introduce the proposed VOF penalization method and then focus on the problem of wall adhesion and contact angle.

2.1. The Volume-Of-Fluid method

In the introduction to this method, we define a modified pressure, p_{rgh}, as follows:

$$p_{rgh} = p - \rho \mathbf{g} \cdot \mathbf{x} \tag{1}$$

where $\mathbf{x}$ is the spatial position vector with respect to the reference pressure point, p the pressure, ρ the density and $\mathbf{g}$ the gravity acceleration vector. This change of variable, initially included in the interFoam solver [20], allows to simplify the pressure boundary conditions in the simulations.

In the Volume-Of-Fluid model [3], the two-phase flow problem is solved using a unique set of incompressible Navier–Stokes equations [21,22], written below using the previously defined working pressure p_{rgh}, i.e.,

$$\rho \frac{\partial \mathbf{u}}{\partial t} + \nabla \cdot (\rho \mathbf{u}\mathbf{u}) = -\nabla p_{rgh} - \mathbf{g} \cdot \mathbf{x} \nabla \rho + \nabla \cdot \left(\mu (\nabla \mathbf{u} + \nabla \mathbf{u}^{\mathbf{T}})\right) + \mathbf{F}_c \tag{2}$$

$$\nabla \cdot \mathbf{u} = 0 \tag{3}$$

where $\mathbf{u}$ is the fluid velocity and where the fluid properties density, ρ, and dynamic viscosity, μ, depend on the indicator function, α, which represents the volume fraction of fluid 1 in each grid cell, through simple mixture relationships:

$$\rho = \alpha \rho_1 + (1 - \alpha)\rho_2 \tag{4}$$

$$\mu = \alpha \mu_1 + (1 - \alpha)\mu_2 \tag{5}$$

We should note that Eqs. (4) and (5) do not necessarily represent an actual physical fluid behavior. This interphase approach could lead to physical inconsistencies if the diffused interphase plays an important role in the flow physics (for instance very thin film drainage, etc.). However, it is commonly used in the case of the VOF model for immiscible fluids because the indicator function is used only, in this case, as a numerical means to deal with the interphase discontinuity. The interface is then transported using the following advection equation called the "VOF equation":

$$\frac{\partial \alpha}{\partial t} + \mathbf{u} \cdot \nabla \alpha = 0 \tag{6}$$

The capillary force, $\mathbf{F}_c$, in Eq. (2), is defined as a volume force [23] and depends on $\nabla\alpha$ such as

$$\mathbf{F}_c = \sigma (\nabla \cdot \mathbf{n}_\alpha) \nabla \alpha \tag{7}$$

where σ is the interfacial tension between the two fluids and $\mathbf{n}_\alpha$ the normal to the interface defined as follows

$$\mathbf{n}_\alpha = \frac{\nabla \alpha}{|\nabla \alpha|} \tag{8}$$

2.2. The penalized Volume-Of-Fluid method

The computational domain Ω is divided in two parts, the fluid domain Ω_{fluid} and the solid domain Ω_{solid} with $\Sigma_{fluid/solid}$ the surface between the two domains as illustrated in Fig. 1.

The mask function χ, necessary to the penalization method, is defined for each cell i as follows

$$\chi_i = 0 \text{ in } \Omega_{fluid} \tag{9}$$

$$\chi_i = 1 \text{ in } \Omega_{solid} \tag{10}$$

For the proposed method, it is also necessary to define the mask function on each face f of the computational grid cells as

$$\chi_f = 1 \text{ on } \Sigma_{solid/fluid} \tag{11}$$

$$\chi_f = 0 \text{ on all others faces} \tag{12}$$

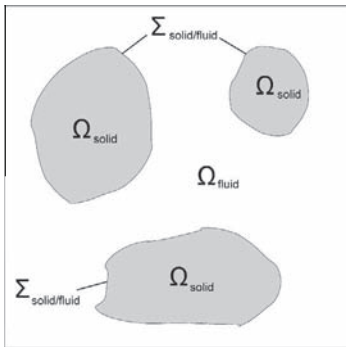

Fig. 1. Schematic representation of the computational domain.

Using the mask function, the momentum Eq. (2) is then modified by adding penalization terms. We write

$$\rho\frac{\partial \mathbf{u}}{\partial t}+\nabla\cdot(\rho\mathbf{u}\mathbf{u})+\chi\frac{\mu}{\kappa_\chi}\mathbf{u}=-\nabla p_{rgh}-(1-\chi)\mathbf{g}\cdot\mathbf{x}\nabla\rho+\nabla\cdot\mu(\nabla\mathbf{u}+\nabla\mathbf{u}^T)+\mathbf{F}_c \tag{13}$$

The first penalization term, $\chi\frac{\mu}{\kappa_\chi}\mathbf{u}$, is inherited from the classical penalization approach applied to the incompressible Navier–Stokes equations [5,11,14]. As demonstrated previously [11], the velocity inside the solid domain is of the order of $\mathcal{O}\left(\left(\frac{\kappa_\chi}{\mu}\right)^{\frac{1}{2}}\right)$. To enforce the no-slip boundary condition at the immersed solid boundaries, the permeability κ_χ must be chosen sufficiently small to reduce the velocity in the solid domain below the numerical error, depending on the algorithm tolerance and the solved problem. The right-hand-side penalization term, $-(1-\chi)\mathbf{g}\cdot\mathbf{x}\nabla\rho$, is necessary to avoid pressure jumps across the immersed boundaries as detailed below in the numerical part.

The transport of the volume fraction is penalized in the solid domain by the no-slip condition already imposed on the velocity field. As it exists a small but non-zero mass flux across immersed boundaries, the convective term in the VOF Eq. (6) should not be penalized to be consistent with the momentum equation. The explicit penalization of the convective term in the VOF equation, for example by imposing a zero flux across immersed boundaries, leads to high instabilities in the numerical simulations. It follows that the volume fraction α in the solid domain has a user-defined fixed value whose influence will be evaluated during the method validation as described in Section 4.

2.3. Wall adhesion and contact angle

The effects of wall adhesion at fluid interfaces in contact with a solid boundary are taken into account by modifying locally the normal to the interface $\mathbf{n}_\alpha$ used in the capillary force formulation [23] (Eq. (7)) as follows

$$\mathbf{n}_\alpha=\mathbf{n}_{wall}\ \cos\theta+\mathbf{n}_t\ \sin\theta \tag{14}$$

where θ is the contact angle, $\mathbf{n}_{wall}$ the normal vector to the wall and $\mathbf{n}_t$ the tangent vector to the wall, in the- direction normal to the contact line. This is numerically done using the following relationship

$$\mathbf{n}_{\alpha,corrected}=\frac{\cos\theta-\cos\theta_I\cos\theta_{diff}}{1-\cos^2\theta_I}\mathbf{n}_{wall}+\frac{\cos\theta_{diff}-\cos\theta_I\cos\theta}{1-\cos^2\theta_I}\mathbf{n}_\alpha \tag{15}$$

where θ_I is the initial angle between $\mathbf{n}_\alpha$ and $\mathbf{n}_{wall}$ and $\theta_{diff}=\theta_I-\theta$. We follow the same technique in our penalization method by expressing the normal to the immersed wall $\mathbf{n}_{i-wall}$ on each face f using the mask function, i.e.,

$$\mathbf{n}_{i-wall,f}=\frac{\chi_f[\nabla\chi]_{c\to f}}{|[\nabla\chi]_{c\to f}|} \tag{16}$$

The operator $[]_{c\to f}$ means that the field values are interpolated from the cell centers to the face centers while the χ_f term is necessary to define the normal $\mathbf{n}_{i-wall,f}$ only on the immersed boundaries. The correction of the interface normal $\mathbf{n}_\alpha$ (Eq. (15)) is then applied to the entire field α and not only to the wall boundaries. We must note that we have a similar treatment for "real" and immersed solid boundaries for the calculation of the wall normals, which allows their coexistence in the same simulation.

3. Numerical method

The numerical implementation of the penalized VOF model is performed using OpenFOAM®, an open source CFD platform suitable for deep modifications of the solved equations. Our approach is based on the OpenFOAM® usual VOF-based solver, called *interFoam*, developed by Rusche [20] and detailed below.

3.1. Advection of the indicator function α

The interface between the two immiscible fluids is represented by a step in the indicator function α, transported with the VOF Eq. (6). Solving numerically a pure advection equation, such as the VOF equation, induces numerical diffusion which tends to smear the interface sharpness. Several strategies have been developed to overcome these numerical issues such as suitable discretization schemes [24,25], interface reconstruction algorithms [26], or the introduction of an artificial compression term as used in the *interFoam* solver [20]. This last approach leads to the following VOF equation, written in the conservative form:

$$\frac{\partial\alpha}{\partial t}+\nabla\cdot(\alpha\mathbf{u})+\nabla\cdot(\alpha(1-\alpha)\mathbf{u}_r)=0 \tag{17}$$

where $\mathbf{u}_r$ is a compression velocity which can be defined in several ways. In the *interFoam* solver, the formulation is based on the maximum velocity magnitude in the transition region, see Rusche[20] for more details. The numerical scheme used for the convective term of the VOF equation is a high resolution scheme with the Van Leer limiter function (second order scheme) and a forward Euler for time discretization. Advection of the indicator function is performed explicitly using the last known velocity field. In order to improve both stability of the simulation and computation time, two different time steps, specified by two different Courant number conditions, are used for the explicitly-solved VOF equation and for the implicitly-solved Navier–Stokes system.

3.2. Pressure–velocity coupling

In the *interFoam* solver, the Navier–Stokes system is solved using an alternative pressure–velocity algorithm based on the PISO algorithm (Pressure Implicit with Splitting Operator) [27]. Predictor–corrector approaches are mainly used to reduce the size of the solved linear systems, and, therefore, the computation time. After discretization, the momentum equation can be written as follows

$$\mathbf{A}_D\mathbf{u}^n=\mathbf{A}_H(\mathbf{u}^n,\mathbf{u}^{n-1})-\nabla p_{rgh}+(1-\chi)\mathbf{g}\cdot\mathbf{x}\nabla\rho+\mathbf{F}_c \tag{18}$$

where $\mathbf{A}_D$ and $\mathbf{A}_H$ are matrix operators (notation commonly used in the OpenFOAM® formalism). $\mathbf{A}_D$ refers to the matrix containing the diagonal entries of the discretized form of the momentum equation, including in our case the penalization term $\frac{\chi}{\mu_\chi}\mathbf{u}^n$. $\mathbf{A}_H$ includes the viscous, inertial, and transient term $\frac{\mathbf{u}^{n-1}}{\Delta t}$, excluding body force, capillary force and pressure gradient. Standard second-order centered schemes are used for the discretization of viscous and inertial terms and a first-order Euler backward scheme for the time derivative.

The momentum Eq. (18) can be reformulated into a flux predictor–corrector equation

$$\phi_f^n=\phi_f^*-(\mathbf{A}_D^{-1}|\mathbf{S}|\nabla p_{rgh})_f \tag{19}$$

where $\mathbf{S}$ is the surface area vector and f means that the values are computed on the mesh faces. The predicted flux field, ϕ_f^*, is computed as follows

$$\phi_f^*=\left(\mathbf{A}_D^{-1}\mathbf{A}_H(\mathbf{u}^k,\mathbf{u}^{n-1})\right)_f\cdot\mathbf{S}+(1-\chi_f)\left(\mathbf{A}_D^{-1}\right)_f|\mathbf{S}|(\mathbf{g}\cdot\mathbf{x}\nabla\rho)_f+|\mathbf{S}|\left(\mathbf{A}_D^{-1}\mathbf{F}_c\right)_f \tag{20}$$

where $\mathbf{A}_H(\mathbf{u}^k,\mathbf{u}^{n-1})$ is computed using the last known velocity field $\mathbf{u}^k$. For the first algorithm iteration, we can use the old-time velocity

field, $\mathbf{u}^{n-1}$, or perform, first, a prediction step by solving the momentum Eq. (2) using the last known pressure field p^{n-1}. We must note at this point that the predicted flux field ϕ_f^* does not satisfy the zero-divergence condition. Then, applying the divergence operator to the flux predictor–corrector flux Eq. (19) and taking into account the zero-divergence condition on the sought flux field ϕ_f^n, the equation can be recast into a Poisson-type equation, called the pressure equation, which reads

$$\nabla \cdot \phi_f^* = \nabla \cdot \left(\left(\mathbf{A}_D^{-1} \right)_f |\mathbf{S}| \nabla p_{rgh} \right) \tag{21}$$

The pressure field obtained by solving the pressure equation can then be introduced into the predictor–corrector flux Eq. (19) to calculate the new flux ϕ_f^n. Issa [27] showed that a minimum of two correction steps are necessary and sufficient for most cases, in order to obtain velocity and pressure fields that can be legitimately considered as solutions to the Navier–Stokes equations. In the case of the *interFoam* solver, three iterations of the presented algorithm are usually performed for each time step.

The penalization term $(1-\chi_f)\mathbf{g}\cdot\mathbf{x}\nabla\rho$, in the predicted flux field Eq. (20), allows to impose a zero flux condition across an immersed solid boundary whatever the value of $\nabla\rho$. It is necessary when an interface is present along an immersed solid boundary, i.e., when the volume fraction differs between the solid and the fluid domain (depending on the user-defined initialization of α, see Fig. 2 and Section 2.2).

3.3. Capillary effects

The interfacial tension effect in Eulerian grids can be computed using different approaches: the continuum surface force [23], the sharp surface force [28] or the ghost fluid model [29]. The computation of the capillary forces is one of the major difficulties encountered in the VOF method, firstly, because the diffuse nature of the interface complicates the curvature computation, and, secondly, because it may cause the presence of spurious currents close to the interfaces. The spurious currents may have a great influence, mainly when the flow is occurring at low capillary number, i.e., when the fluids dynamics are capillary-dominated, as observed by Harvie et al. [30]. Previous works have also been conducted on these spurious currents to evaluate their magnitude [31], or to study the influence of various simulation parameters [32]. A recent study [19] developed a stable numerical scheme, based on sharp representation of the surface tension coupled with filtering methods, which allows to simulate flow in porous media where the characteristic size is of the order of millimeters. In this study, we keep the usual procedure of the continuum representation described by Brackbill et al. [23].

As explained in Section 2.2, the α-field has a fixed value in the solid domain (see an example in Fig. 2), which may have an influence on the capillary effect computation at and near immersed boundaries. Contrary to a real solid boundary, $\nabla\alpha$ across an immersed solid boundary is not necessarily equal to zero and may affect locally the curvature computation in Eq. (7).

The curvature computation in the VOF method is challenging because we usually try to keep the interface over a few cells, using some compression algorithms, which may lead to inaccuracy on the direction of the normal to the interface, $\mathbf{n}_\alpha$. To improve the interface curvature computation, the α-field used in the interface normal computation (Eq. (8)) can be smoothed by successive linear interpolations (two interpolations in our simulations) between cell centers and face centers (previous studies have successfully performed similar operations [19,33–35]):

$$\alpha_{k+1} = C_S \left[[\alpha_k]_{c\to f} \right]_{f\to c} + (1-C_S)\alpha_k \tag{22}$$

where C_S is a smoothing coefficient whose value is discussed in the numerical validation. The operator $[]_{c\to f}$ means that the field values are interpolated from the cell centers to the face centers while the operator $[]_{f\to c}$ means the inverse operation. In our model, the smoothing operation may have a strong influence on the simulation results, which is mainly due to the specific shape of the interface close to the immersed boundaries (see Fig. 2).

Previous studies [19,36] reported that implementing a contact angle condition on complex solid boundaries without smoothing operations on the normal to the walls could lead to large spurious velocities. A smoothing operation is therefore applied to the $\nabla\chi$-field in the computation of the normal to the immersed wall $\mathbf{n}_{i-wall,f}$ (Eq. (16)) using the following equation:

$$(\nabla\chi)_{f,k+1} = \chi_f \left[\left[(\nabla\chi)_k \right]_{f\to c} \right]_{c\to f} \tag{23}$$

For each linear interpolation iteration, the $\nabla\chi_f$-field is multiplied by χ_f to keep the normal $\mathbf{n}_{i-wall,f}$ on the immersed solid boundaries. A schematic representation of the smoothing operation is depicted in Fig. 3.

A preliminary study on the penalization method showed that modifying the normal to the interface at the immersed boundaries (to take into account the wall wettability) makes the method conditionally unstable, highly dependent on the α_{solid} initialization (cf Fig. 2). The presence of the interface along the immersed solid boundary affects the interface curvature computation and leads to overestimation of the capillary force. This error depends on the contact angle and reaches its maximum value for the largest local interface curvature, i.e., when the contact angle tends to 90°. Moreover, in case of a curved immersed solid boundary, the curvature of the interface along the immersed wall is different

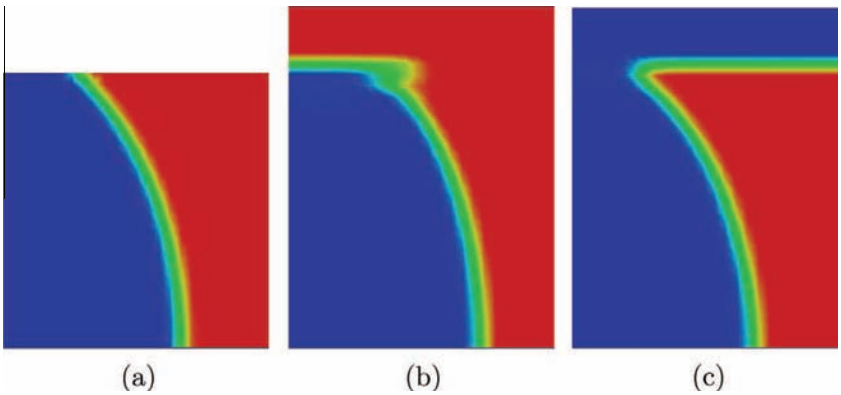

Fig. 2. Contact line visualization for different methods: (a) VOF method, (b) penalized VOF with $\alpha_{solid} = \alpha_{gas}$, (c) penalized VOF with $\alpha_{solid} = \alpha_{liquid}$.

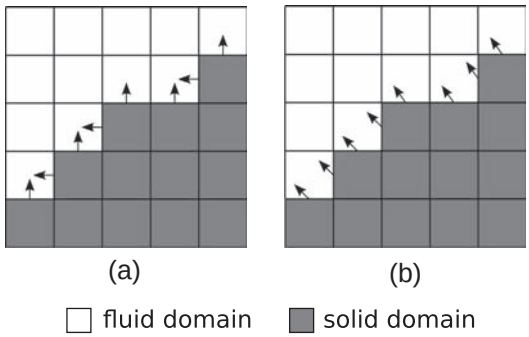

Fig. 3. Different representations of the normal to the immersed walls $\mathbf{n}_{wall,immersed}$: (a) no smoothing, (b) with smoothing.

from zero, which may induce a non-physical capillary pressure between the solid and the fluid domain.

To overcome this numerical issue, the momentum prediction Eq. (20) is modified by expanding the penalization term to the capillary force term. We write

$$\phi_f^* = \left(\mathbf{A}_D^{-1}\mathbf{A}_H(\mathbf{u}^k,\mathbf{u}^{n-1})\right)_f \cdot \mathbf{S} + (1-\chi_f)\left[\left(\mathbf{A}_D^{-1}\right)_f |\mathbf{S}|\mathbf{g}\cdot(\mathbf{x}\nabla\rho)_f + |\mathbf{S}|\left(\mathbf{A}_D^{-1}\cdot\mathbf{F}_c\right)_f\right] \tag{24}$$

This term cancels out all fluxes depending on $\nabla\alpha$ along the immersed boundaries, which reduces the possible influence of an interface along the wall. The wettability is then taken into account by modifying the interface normal on the adjacent face close to the immersed boundary, as depicted in Fig. 4. This wettability shift is simply done by modifying the wall-smoothing operation (23) for the last iteration k_{last} as follows

$$(\nabla\chi)_{k_{last}} = \left[\left[(\nabla\chi)_{k_{last}-1}\right]_{f\to c}\right]_{c\to f} \tag{25}$$

which provides a $\mathbf{n}_{wall,immersed,f}$-field defined on the faces adjacent to the immersed boundaries. Note that the volume penalization term remains on the *solid* cells, which induces a *shifting* between no-slip and wettability boundary conditions.

4. Numerical validation

In this section, several test cases are solved using the proposed method and the approach is validated by comparing the numerical results with analytical results or with a reference solution, i.e., the one obtained from the usual VOF-based solver*interFoam*. Fluids used for the following tests are air ($\rho = 1.225$ kg m^{-3}, $\mu = 1.78 \times 10^{-5}$ Pa s) and water ($\rho = 980$ kg m^{-3}, $\mu = 1.0 \times 10^{-3}$ Pa s) under atmospheric conditions. The interfacial tension, σ, between the two fluids is 0.073 N m^{-1}. The characteristic length chosen for the tested geometries is close to the capillary length, i.e., of the order of a millimeter, because the capillary-dominated flows represent one of the most sensitive cases for VOF simulations (see Section 3.3). Validating the presented method on capillary-dominated flows ensures that immersed wall effects in the penalized method are correctly taken into account and, therefore, that the approach is valid in a more general way. For the following simulations, we set $\kappa_\chi = 10^{-30}$ m^2 and algorithm tolerance equal to 10^{-7} for p and $\mathbf{u}$. In these conditions, the velocity field inside the solid is negligible, i.e., its magnitude is lower than numerical accuracy.

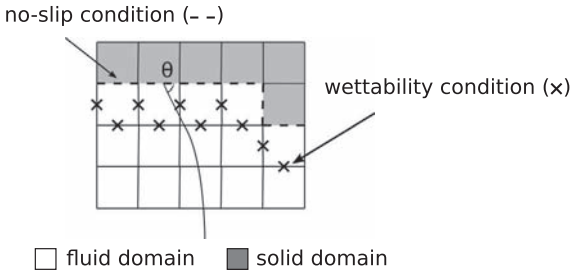

Fig. 4. Schematic representation of the shift between the no-slip condition and the wettability condition.

The method is first validated in two simple cases: a circular drop at equilibrium and the displacement of a meniscus in a simple Hele-Shaw cell. Then, an obstacle is placed in the cell to observe the behavior of the method in the presence of a solid boundary with a more complex shape. Finally, the method is used to simulate the impact of a droplet on a solid support.

4.1. Circular drop at equilibrium

The first case studied is a two-dimensional drop at equilibrium on a wetting or non-wetting plane surface. The configuration is exactly similar to the work of Dupont and Legendre [35]. The initial volume of the drop is πR_0^2 with reference radius $R_0 = 1$ mm. The contact angle varies from $\theta = 10$ to 170° and the real radius R of the drop is therefore given by:

$$R = R_0\sqrt{\frac{\pi}{\theta - \sin\theta\cos\theta}} \tag{26}$$

while the pressure jump across the interface is computed by Laplace's law:

$$\Delta p_{analytical} = \frac{\sigma}{R} \tag{27}$$

For each configuration tested ($\theta = 10°, 30°, 60°, 90°, 120°, 150°, 170°$), the initial condition is the exact solution, i.e., a drop whose width is given by $L_{drop} = 2R \times \sin\theta$ and height by $H_{drop} = R \times (1 - \cos\theta)$. The size of the Cartesian grid spacing is defined so that the drop height contains 40 cells (similar to the work previously cited [35]). The corresponding mesh has between 6480 ($\theta = 170°$) and 146,320 ($\theta = 10°$) computation cells. For the penalized approach, five cells are added on the bottom of the simulation domain to represent the plane surface as a fine penalized layer. Fig. 5 shows the initial condition for the 3 methods: usual VOF, $\alpha_{solid} = \alpha_{liquid}$ and $\alpha_{solid} = \alpha_{gas}$.

For all the penalized configurations, simulations are performed with and without smoothing operation ($C_S = 0$ or 0.5). The numerical validation is evaluated in terms of the averaged pressure inside the drop, which is numerically calculated as follows:

$$\Delta p = \frac{\int_V (1-\chi)\alpha p \, dV}{\int_V (1-\chi)\alpha \, dV} - p_{out} \tag{28}$$

with the reference pressure $p_{out} = 0$. Fig. 6 shows the results obtained with $\alpha_{solid} = \alpha_{gas}$ and $\alpha_{solid} = \alpha_{liquid}$. Note that, in this Figure, the absence of value for one method means that the drop is unstable in that case, i.e., that pressure and velocity fields are oscillating. This is the case for $\theta < 90°$ (liquid wetting) and $\alpha_{solid} = \alpha_{gas}$ (Fig. 6b) and also for $\theta > 90°$ (gas wetting), $\alpha_{solid} = \alpha_{liquid}$, and $C_S = 0$ (Fig. 6b).

One should note that the difference between theoretical results and the usual VOF is of the order of 10% for the various contact angles tested and that it is due to the current implementation of the VOF method in the OpenFOAM® software. More accurate simulations would require specific recent improvements, such as capillary forces smoothing and filtering [19,35], that are not in the scope of this paper and not available in the CFD tool used. For stable configurations, numerical results obtained with the penalized approach are close to those obtained with the standard VOF method. Smoothing operation has a small influence except

Fig. 5. Initial conditions ($\theta = 60^\circ$) for the different methods: (a) usual VOF, (b) $\alpha_{solid} = \alpha_{liquid}$, (c) $\alpha_{solid} = \alpha_{gas}$.

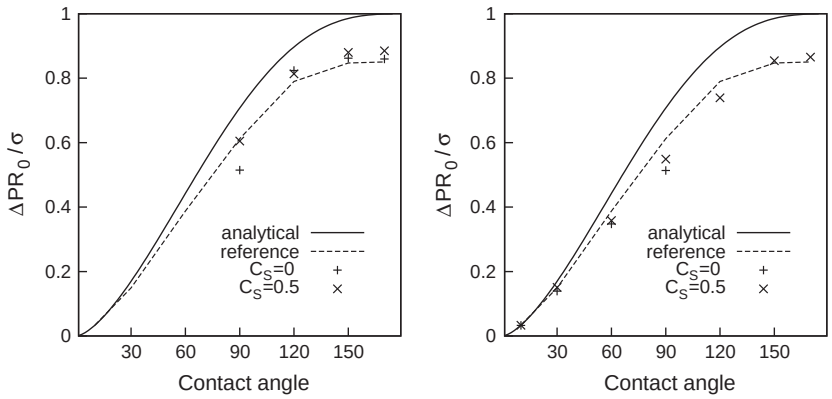

Fig. 6. Pressure inside the drop versus the contact angle: (a) $\alpha_{solid} = \alpha_{gas}$, (b) $\alpha_{solid} = \alpha_{liquid}$.

for high curvatures close to the immersed boundaries, i.e., when $\theta \to 90^\circ$. The most accurate results are obtained by initializing the immersed boundaries with the wetting fluid and using the smoothing function ($C_S = 0.5$). For the particular intermediate case, $\theta = 90^\circ$, the best agreement is found for $\alpha_{solid} = \alpha_{gas}$.

A mesh sensitivity study is performed for the case $\theta = 60^\circ$ ($\alpha_{solid} = \alpha_{liquid}$) and the relative differences between penalized method results and the usual VOF results are reported in Fig. 7a for three mesh characteristic sizes. We can observe that the additional numerical error induced by the penalized approach is of the order 1/2. As the usual VOF method has an order of convergence of 1, we can conclude that the global order of convergence of the penalized method is at most 1/2. The parasitic currents, i.e., the maximal velocity magnitude, is plotted in Fig. 7b as a function of temporal iterations for the different methods (with $\theta = 60^\circ$ and $\Delta x = \Delta y = \frac{H_{drop}}{40}$). The instability of the "unwetted" simulations is illustrated by higher values of parasitic currents while the "wetted" approaches show similar magnitudes as the usual VOF method.

4.2. Capillary displacements in a Hele-Shaw cell

We now study a dynamic case, e.g. the capillary displacements into an Hele-Shaw cell to observe the method behavior when the contact line is moving. We consider a horizontal Hele-Shaw cell (width = 1 mm and length = 10 mm) with a computational grid, for the reference case, composed of 25×500 cells with a characteristic size 20 by 20 μm. In the case of the penalized method, the simulations are performed using an Hele-Shaw cell with a spacing of 1.2 mm while defining the immersed solid domain as a layer of thickness of 0.1 mm along the wall, as depicted in Fig. 8. The computational grid for this method is composed of 30×500 cells which induces the same discretization of the fluid domain. Boundary conditions are fixed pressure on both sides. By varying the contact angle θ, it is possible to change the capillary pressure and, therefore, the meniscus velocity. Simulation conditions are summarized in Fig. 8.

The simulations are performed for $\theta \in [10^\circ, 80^\circ]$, $\alpha_{solid} = \alpha_{liquid}$ or α_{gas}, and for $C_S = 0$ or 0.5.

4.2.1. Spontaneous capillary invasion

The Hele-Shaw is initially filled with the non-wetting fluid and the same pressure is imposed on both sides. Under such conditions, the meniscus behavior is only controlled by capillary pressure. Numerical results obtained for a solid domain initialized with the wetting fluid ($\alpha_{solid} = \alpha_{liquid}$) in that configuration are plotted in Fig. 9. Note that in the following figures, time is normalized by

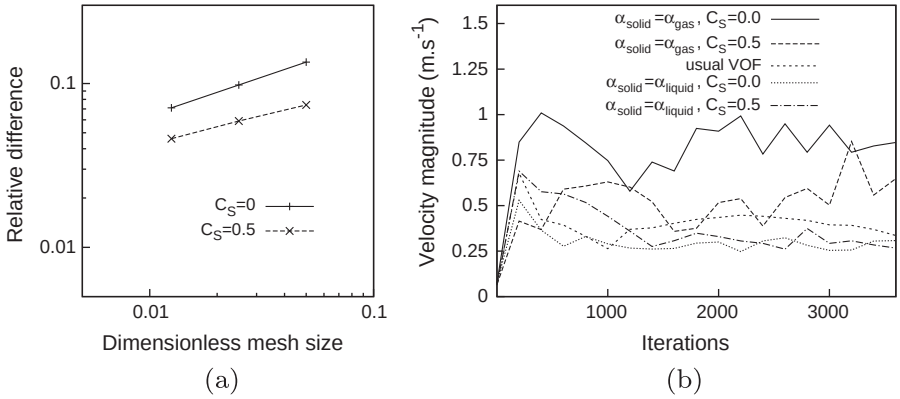

Fig. 7. (a) Relative difference between penalized approaches and usual VOF $\left(\frac{||\Delta p_{penalized} - \Delta p_{usual}||}{\Delta p_{usual}}\right)$ as a function of dimensionless mesh size $\left(\frac{\Delta x}{H_{drop}}\right)$ between the penalized approaches ($\alpha_{solid} = \alpha_{liquid}$) and the usual VOF method. (b) Parasitic currents (velocity magnitude) as a function of temporal iterations for the different configurations $\left(\Delta x = \Delta y = \frac{H_{drop}}{40}\right)$.

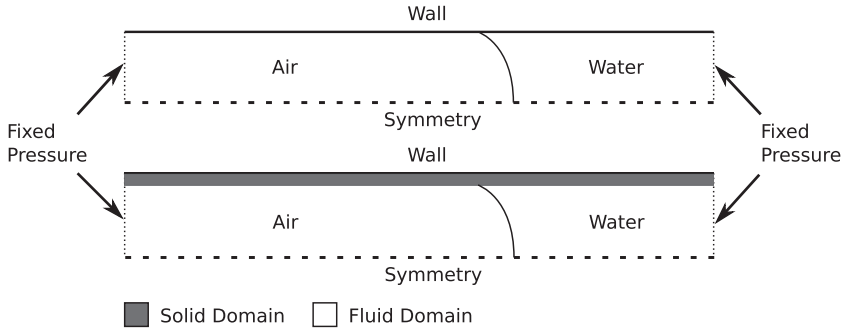

Fig. 8. Simulation conditions for the usual VOF method (top) and the penalized VOF method (bottom).

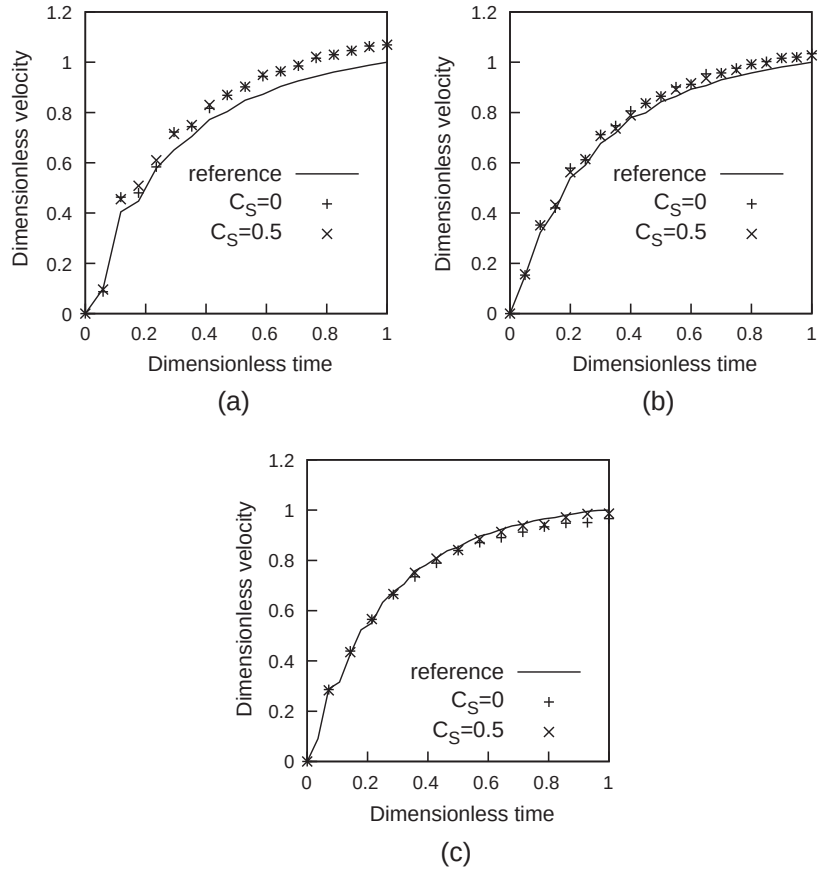

Fig. 9. Meniscus velocity as a function of time with $\alpha_{solid} = \alpha_{liquid}$: (a) $\theta = 10°$, (b) $\theta = 40°$, (c) $\theta = 70°$. Velocities are made dimensionless by the maximal reference velocity (respectively, $V_{meniscus,ref} = 6.01 \times 10^{-1}, 5.48 \times 10^{-1}$ and 3.66×10^{-1} m s^{-1}).

the final time of the reference simulation, i.e., when the meniscus leaves the computational domain. The figure shows the velocity (made dimensionless by the maximal reference velocity) of the interface, equal to zero at $t = 0$, as a function of time for three cases: $\theta = 10°$, $40°$ and $70°$. For the whole range of contact angles tested, numerical results obtained with $C_S = 0$ and $C_S = 0.5$ are very close, which confirms the observations of Section 4.1, i.e., that the smoothing coefficient C_S has a small influence on the simulations. The comparison between the penalized and the usual approach shows a maximum relative difference in terms of meniscus velocity of 6.9% for $\theta = 10°$, 3.4% for $\theta = 40°$ and 3.2% for $\theta = 70°$. This figure shows that the penalized approach tends to slightly underestimate the contact angle, which is particularly visible for the lowest contact angles, i.e., $\theta = 10°$ in Fig. 9.

Simulations are then performed with $\alpha_{solid} = \alpha_{gas}$ and the numerical results are plotted in Fig. 10. First, this figure shows that, contrary to the case $\alpha_{solid} = \alpha_{liquid}$, the smoothing coefficient has a non-negligible influence on the results. In the case with no-smoothing ($C_S = 0$), the capillary effects are overestimated and the maximum relative difference oscillates between 6% for $\theta = 70°$ and 9.9% for $\theta = 10°$. On the opposite, simulations with $C_S = 0.5$ show an underestimation of the capillary effects with a maximum difference between 0.6% for $\theta = 10°$ and 35.3% for $\theta = 70°$. We attribute this strong influence of the smoothing coefficient, C_S, to the shape of the interface in the case with $\alpha_{solid} = \alpha_{gas}$, which presents an important curvature close to the immersed boundary (see Fig. 2). At this point, and in accordance to the findings of Section 4.1, the "wetting solid" approach

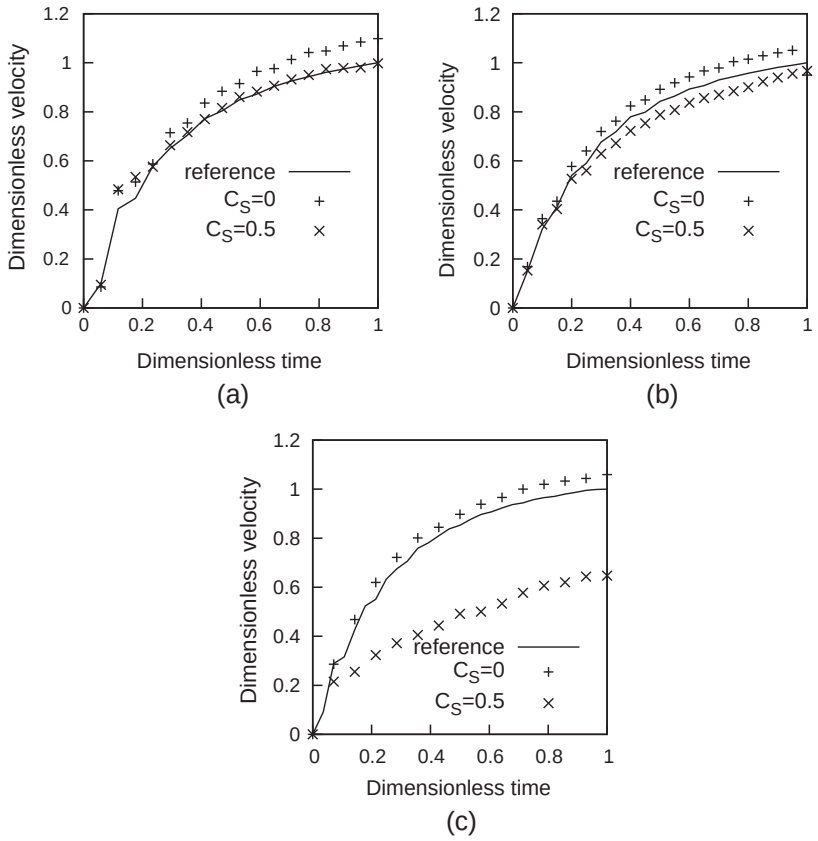

Fig. 10. Meniscus velocity as a function of time with $\alpha_{solid} = \alpha_{gas}$: (a) $\theta = 10°$, (b) $\theta = 40°$, (c) $\theta = 70°$. Velocities are made dimensionless by the maximal reference velocity (respectively, $V_{meniscus,ref} = 6.01 \times 10^{-1}, 5.48 \times 10^{-1}$ and 3.66×10^{-1} m s^{-1}).

Table 1
Effect of grid size on maximal dimensionless velocity in the Hele-Shaw cell.

Mesh size	Usual VOF	$\alpha_{solid} = \alpha_{liquid}$		$\alpha_{solid} = \alpha_{gas}$	
		$C_S = 0$	$C_S = 0,5$	$C_S = 0$	$C_S = 0,5$
500×30	1.028	1.099	1.099	1.129	1.026
700×42	1.026	1.090	1.096	1.104	1.014
1000×60	1	1.071	1.088	1.081	1.038

($\alpha_{solid} = \alpha_{liquid}$ when $\theta < 90°$) seems to be the best compromise between accuracy and stability. A mesh sensitivity is performed on that case for $\theta = 10°$ and numerical results are summarized in Table 1. The difference between the coarsest and the finest grid results is less than 3% for all the configurations.

4.2.2. Receding meniscus

The Hele-Shaw domain is now initially filled with the wetting fluid and we impose a pressure gradient ($P_{in,air} = 150$ Pa) to observe the inverse displacement of the meniscus in the Hele-Shaw cell.

In the case $\alpha_{solid} = \alpha_{gas}$, the dimensionless meniscus velocity versus time is represented Fig. 11 for three different contact angles. The reference solution is compared with the penalized method with $C_S = 0$ and $C_S = 0.5$. The figure shows a non-negligible difference between the penalized approach and the reference solution, for the entire series of tests. Moreover, in the case $\theta = 10°$, the meniscus establishment lead to front velocity oscillations which persist when $C_S = 0$. The $\alpha-$smoothing operation tends to reduce these oscillations, but also increases the velocity difference with the reference solution (from 11.1% with $C_S = 0$ to 21.9% with $C_S = 0.5$). Findings are similar for larger contact angles: the $\alpha-$smoothing provides a better stability but also a greater inaccuracy of the numerical simulations. The minimum difference in the case $\alpha_{solid} = \alpha_{gas}$, is 10.9% and is reached with $C_S = 0$ and $\theta = 70°$.

Numerical results with $\alpha_{solid} = \alpha_{liquid}$ are plotted in Fig. 12. The figure shows a good agreement in terms of meniscus velocity between the various penalized simulations and the reference solution. The maximum difference, equal to 9.6%, is reached for $C_S = 0.5$ and $\theta = 10°$. The interface velocity oscillations, previously observed in the case $\alpha_{solid} = \alpha_{gas}$, are not present when the immersed solids are flooded with the wetting fluid. However, the α-smoothing procedure still increases the velocity difference with the reference case, but to a lesser extent than in the case where $\alpha_{solid} = \alpha_{gas}$, as depicted in Fig. 12. Numerical results with $\alpha_{solid} = \alpha_{liquid}$ show the best agreement with the reference solution, for a wide range of contact angles, with a relative difference less than 2.9% while the smoothing coefficient has a small influence.

In conclusion to this Hele-Shaw cell study, it appears that filling the solid domain with the wetting fluid provides more stable and accurate simulations without adjustable parameters, contrary to the configuration with $\alpha_{solid} = \alpha_{gas}$ which has an efficiency and accuracy highly dependent from the studied case.

4.3. Hele-Shaw cell with obstacle

The penalized method is then tested in the case of a receding meniscus within a Hele-Shaw cell with different obstacles. We first study the meniscus displacement in a Hele-Shaw cell (dimensions: 1×5 mm, $P_{in,air} = 150$ Pa, $\theta = 45°$) containing an obstacle with a rectangular shape (0.4×3 mm). A comparison of the interface configurations at a given time between usual and penalized VOF

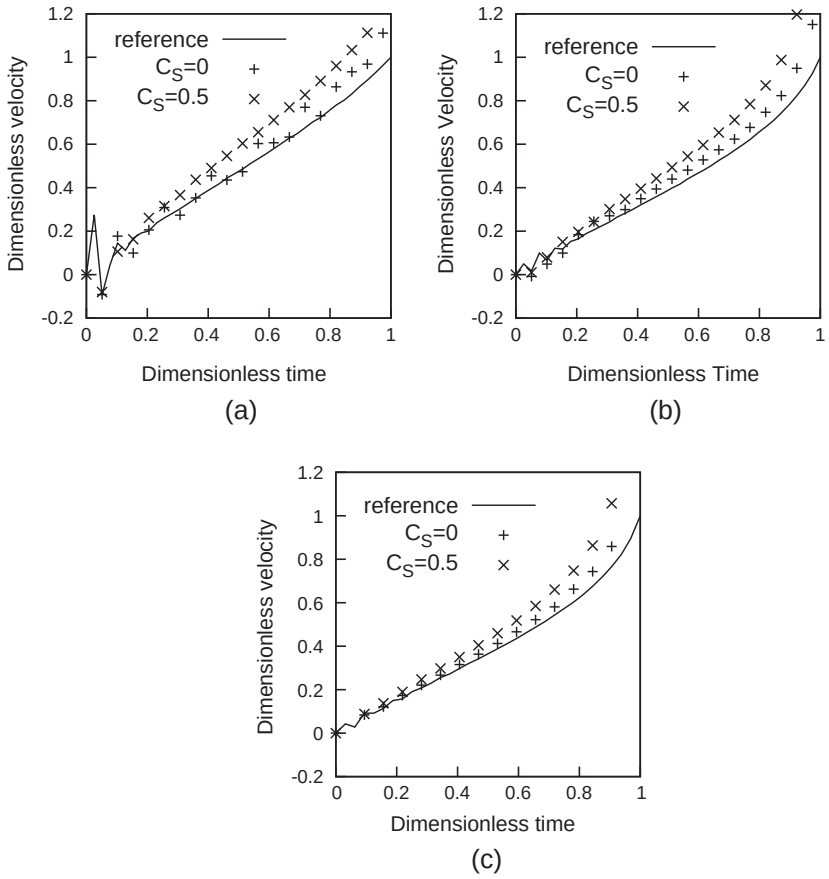

Fig. 11. Meniscus velocity as a function of time with $\alpha_{solid} = \alpha_{gas}$: (a) $\theta = 10°$, (b) $\theta = 40°$, (c) $\theta = 70°$. Velocities are made dimensionless by the maximal reference velocity (respectively, $V_{meniscus.ref} = 2.80 \times 10^{-1}, 4.70 \times 10^{-1}$ and 2.64×10^{-1} m s^{-1}).

simulations is shown in Fig. 13a. As in the case of the meniscus displacement in a Hele-Shaw cell, we validate the penalization approach by a comparison with the reference solution in terms of meniscus velocity (see Fig. 14). The figure confirms the findings of the Hele-Shaw cell study with a receding meniscus. The case $\alpha_{solid} = \alpha_{gas}$ fails to simulate correctly the meniscus behavior. Increasing the α-smoothing operation ($C_S = 0.5$) provides a better stability at the expense of a larger inaccuracy. The best agreement is found for $\alpha_{solid} = \alpha_{liquid}$, i.e., the same configuration used for the simple Hele-Shaw case studied in Section 4.2.1.

The second test consists of an Hele-Shaw cell containing an obstacle with curved boundaries, i.e., not aligned with the mesh. A comparison of interface configurations at a given time between usual and penalized VOF simulations is presented in Fig. 13b. The figure shows a good agreement between usual and penalized VOF in terms of meniscus position, as for the cases described above.

This case allows to emphasize the impact of the smoothing of the normal to the immersed wall $\mathbf{n}_{wall.immersed}$, detailed in section 3.3, and illustrated in Fig. 15 (right). The comparison with the reference solution (Fig. 15b) shows a better agreement when the normal to the immersed wall is smoothed (Fig. 15c).

4.4. 3D Droplet impact

We now study a droplet impact on a flat solid surface, a situation known to feature different dynamic behaviors [37–39], depending on the adopted physical conditions such as, for example, the wetting conditions. The configuration is similar to the experimental study of Wang et al. [39], i.e., the normal collision of a water droplet (diameter $d = 2$ mm) with an initial velocity $V_{droplet} = 0.517$ m s^{-1} on hydrophilic (glass) or hydrophobic (paraffin) surfaces. The size of the computational domain is $6 \times 6 \times 2.5$ mm, and, to reduce the computational domain, we simulate a quarter of the droplet by considering two symmetry planes. The computational grid is regular and composed of $60 \times 32 \times 60$ cells ($\Delta x = \Delta y = \Delta z = \frac{d}{40}$).

We focus the study on the hydrophobic case where the contact angle has been measured experimentally and varies non-regularly between 80° and 120°, depending on the moving contact line. In the numerical calculations, we set a constant contact angle $\theta = 100°$ and perform numerical simulations with the penalized approach and the two choices: $\alpha_{solid} = \alpha_{gas}$ and $\alpha_{solid} = \alpha_{liquid}$. Interface profiles are plotted in Fig. 16 at different time steps: $t = 1, 5, 10, 15, 20, 29 \times \tau$ with $\tau = \frac{1}{2905}$ s. This corresponds to the time interval between two images of the study of Wang et al. [39] and numerical results can therefore be directly compared with Fig. 5 of the previously cited paper. The two simulations ($\alpha_{solid} = \alpha_{gas}$ and $\alpha_{solid} = \alpha_{liquid}$) are almost similar and numerical results are in good agreement with the experimental visualizations. The penalized VOF method reproduces the different stages of the droplet impact on an unwetting surface, i.e., the spreading of the drop (Fig. 16a,b,c), followed by the formation of a liquid ring (Fig. 16d,e), which then leads to a fast growth of a central cone (Fig. 16f). We should note that the last stage, the fast growth, is slower in the numerical simulation which may be due to the static angle assumption (which is dynamic in the real case) but also to the coarse mesh used. Indeed, it has been shown in Section 4.1 that a mesh with a characteristic size of $\frac{h_{drop}}{20}$ may lead to an underestimation of the capillary effects of about 8 %. The capillary effect

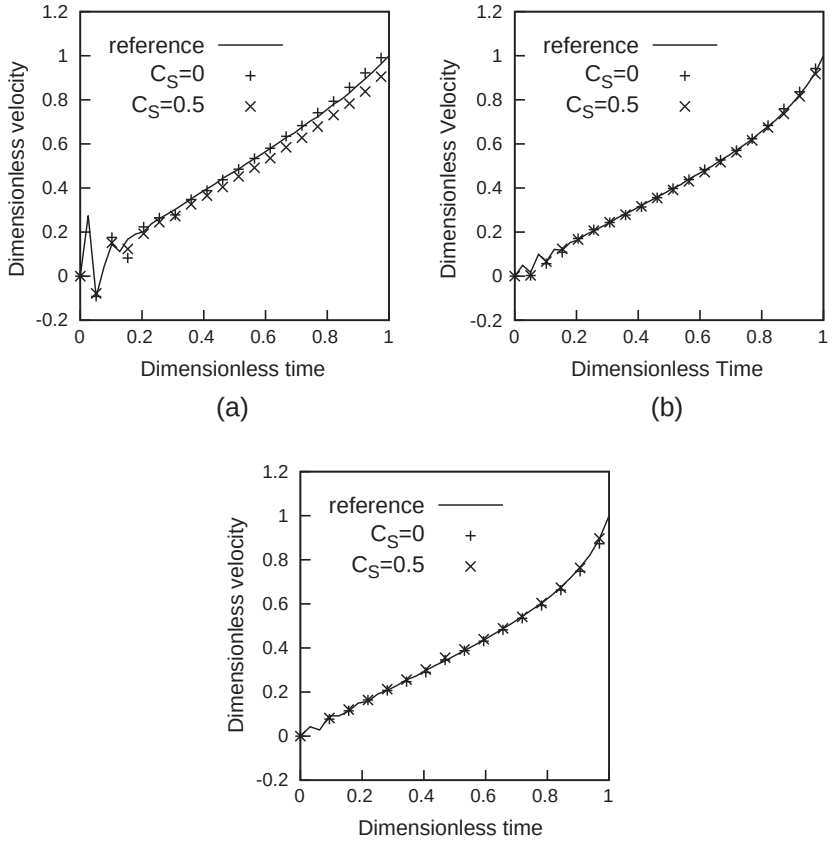

Fig. 12. Meniscus velocity as a function of time with $\alpha_{solid} = \alpha_{liquid}$: (a) $\theta = 10°$, (b) $\theta = 40°$, (c) $\theta = 70°$.Velocities are made dimensionless by the maximal reference velocity (respectively, $V_{meniscus.ref} = 2.80 \times 10^{-1}, 4.70 \times 10^{-1}$ and 2.64×10^{-1} m s^{-1}).

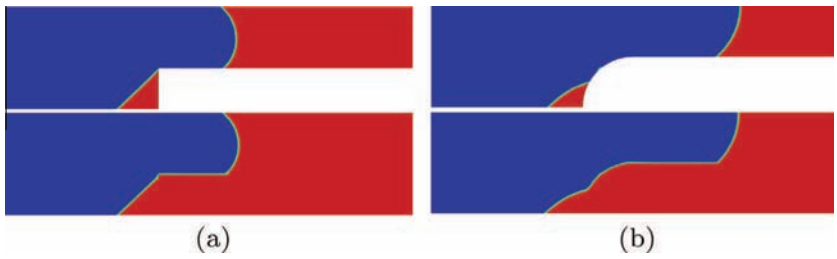

Fig. 13. Two-phase flow in a Hele-Shaw cell with a rectangular-shaped (a) or curved-shaped (b) obstacle (top: usual VOF, bottom: penalized VOF).

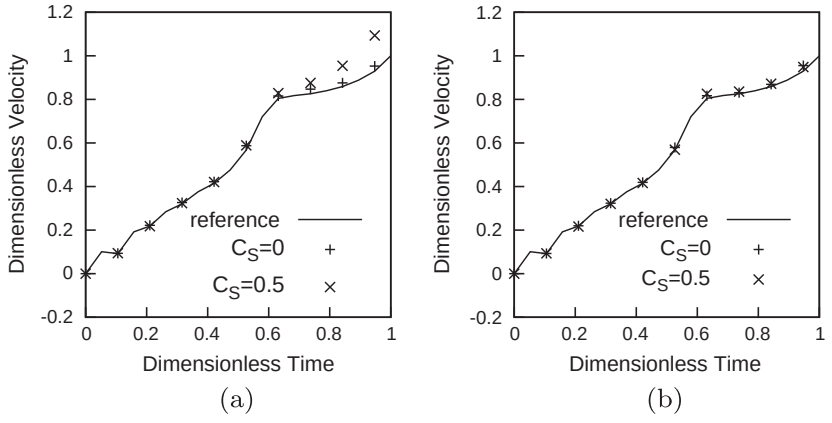

Fig. 14. Meniscus velocity as a function of time for the Hele-Shaw cell with an obstacle: (a) $\alpha_{solid} = \alpha_{gas}$, (b) $\alpha_{solid} = \alpha_{liquid}$.

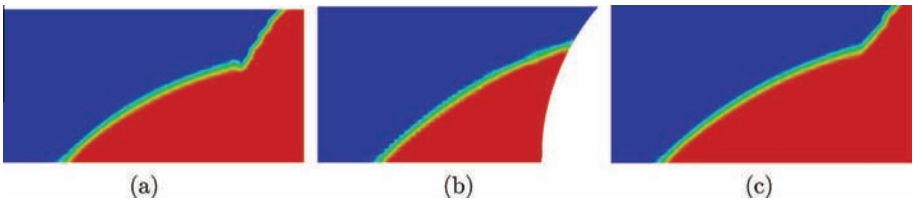

Fig. 15. Simulation of the wettability condition on a curved wall: (a) $\mathbf{n}_{wall,immersed}$ non-smoothed, (b) reference solution, (c) $\mathbf{n}_{wall,immersed}$ smoothed.

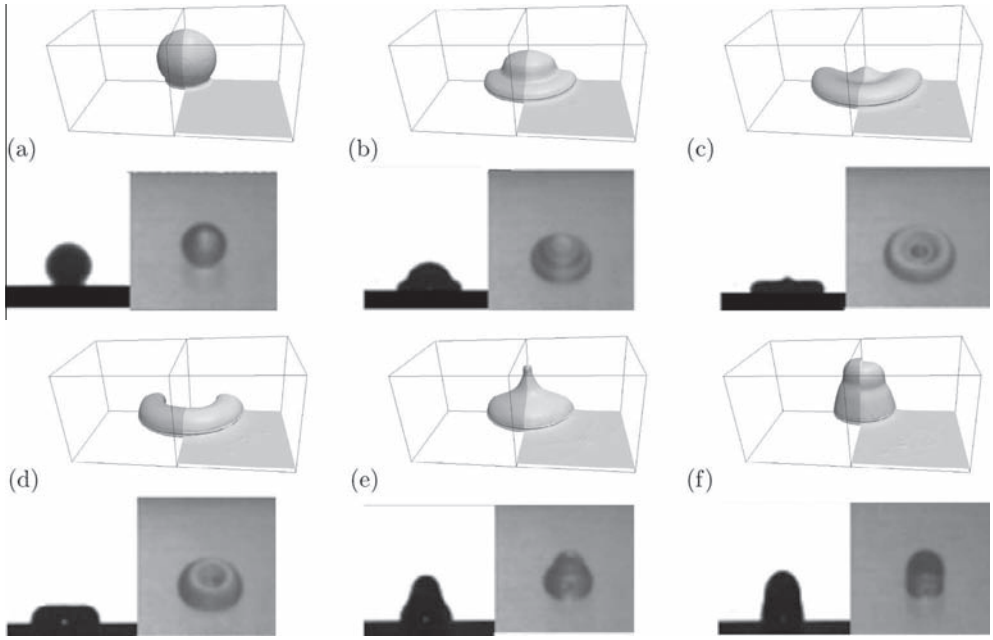

Fig. 16. Visualization of the interface dynamics of a droplet impact at different time steps ($t = 1, 5, 10, 15, 24, 29 \times \tau$ with $\tau = \frac{1}{2905}$ s) for two penalized approaches: $\alpha_{solid} = \alpha_{gas}$ (left) and $\alpha_{solid} = \alpha_{liquid}$ (right). Numerical results are compared with experimental visualizations from Wang et al. [39].

difference, and therefore the time shift between simulations and visualizations, can be probably reduced by refining the mesh. The case with $\alpha_{solid} = \alpha_{gas}$ is slightly closer to the experimental visualization, which confirms that initializing the solid domain with the wetting phase provides more accurate results.

5. Conclusions

We developed in this paper a penalization approach applied to the "Volume-Of-Fluid" method to simulate two-phase flows with the presence of immersed solid boundaries. A special attention has been given on the wettability condition on the immersed boundaries, which, through the presence of an interface along the immersed boundaries, may trigger instabilities in the numerical simulations and inaccuracy in the capillary forces computation. By separating the no-slip condition with the wettability condition, the method developed is stable for all cases tested and almost independent from the initial conditions in the solid domain. However, this study showed that initializing the α-field (the solid phase indicator) in the solid domain with the wetting fluid reduces the potential effect of the*immersed curvature* (higher when solid domain is *unwetted*) and allows to simulate two-phase flows *without adjustable parameters*, for a wide range of cases with a good accuracy provided a sufficiently refined mesh is used. To evaluate numerical errors induced by the method, the validation study has been performed on various cases of capillary-dominated flows, driven by the wall effects. Numerical validation has been performed on several 2D cases and the 3D numerical simulations of a drop impact on a flat surface have been favorably compared with experimental visualizations. The proposed penalized method can thus be used with confidence provided that the mesh refinement is adapted to the importance of wetting effects.

References

[1] Sussman M, Smereka P, Osher S. A level-set approach for computing solutions to incompressible two-phase flow. J Comput Phys 1994;114:146–59.
[2] Cahn JW, Hilliard JE. Free energy of a nonuniform system. I. Interfacial free energy. J Chem Phys 1958;28(2):258.
[3] Hirt CW, Nichols BD. Volume-of-Fluid method for the dynamics of free boundaries. J Comput Phys 1981;39:201–25.
[4] Peskin CS. Numerical analysis of blood flow in the heart. J Comput Phys 1977;25(3):220–52.
[5] Peskin CS. The fluid dynamics of heart valves: experimental, theoretical, and computational methods. Annu Rev Fluid Mech 1982;14(1):235–59.
[6] Cheny Y, Botella O. The LS-STAG method: a new immersed boundary/level-set method for the computation of incompressible viscous flows in complex moving geometries with good conservation properties. J Comput Phys 2010;229(4):1043–76.
[7] Mittal R, Dong H, Bozkurttas M, Najjar FM, Vargas A, Von Loebbecke A. A versatile sharp interface immersed boundary method for incompressible flows with complex boundaries. J Comput Phys 2008;227(10):4825–52.
[8] Peskin CS. The immersed boundary method. Acta Numer 2002;11:479–517.
[9] Mittal R, Iaccarino G. Immersed boundary methods. Annu Rev Fluid Mech 2005;37(1):239–61.
[10] Saiki E, Biringen S. Numerical simulation of a cylinder in uniform flow: application of a virtual boundary method. J Comput Phys 1996;123(2):450–65.
[11] Angot P, Bruneau C, Fabrie P. A penalization method to take into account obstacles in incompressible viscous flows. Numer Math 1999;81(4):497–520.
[12] Schneider K, Farge M. Decaying two-dimensional turbulence in a circular container. Phys Rev Lett 2005;95(24):244502.
[13] Liu Q, Vasilyev OV. A Brinkman penalization method for compressible flows in complex geometries. J Comput Phys 2007;227(2):946–66.

[14] Kadoch B, Kolomenskiy D, Angot P, Schneider K. A volume penalization method for incompressible flows and scalar advection–diffusion with moving obstacles. J Comput Phys 2012;231(12):4365–83.
[15] Prodanović M, Bryant SL. A level set method for determining critical curvatures for drainage and imbibition. J Colloid Interface Sci 2006;304(2):442–58.
[16] Vincent S, Sarthou A, Caltagirone J-P, Sonilhac F, Février P, Mignot C, et al. Augmented Lagrangian and penalty methods for the simulation of two-phase flows interacting with moving solids: application to hydroplaning flows interacting with real tire tread patterns. J Comput Phys 2011;230(4):956–83.
[17] Jettestuen E, Helland JO, Prodanović M. A level set method for simulating capillary-controlled displacements at the pore scale with nonzero contact angles. Water Resour Res 2013. n/a–n/a.
[18] Guillaument R, Vincent S, Caltagirone J-P, Laugier M, Gardin P. A new volume of fluid model for modeling wetting effects. application to the impact of emulsion o/w droplets on a moving plate. In: 7th Int. conf. multiph. flow; 2011.
[19] Raeini AQ, Blunt MJ, Bijeljic B. Modelling two-phase flow in porous media at the pore scale using the Volume-Of-Fluid method. J Comput Phys 2012;231(17):5653–68.
[20] Rusche H. Computational fluid dynamics of dispersed two-phase flows at high phase fractions. Ph.D. thesis; 2002.
[21] Kataoka I. Local instant formulation of two-phase flow. Int J Multiph Flow 1986;12(5):745–58.
[22] Scardovelli R, Zaleski S. Direct numerical simulation of free-surface and interfacial flow. Annu Rev Fluid Mech 1999;31(1):567–603.
[23] Brackbill JU, Kothe DB, Zemach C. A continuum method for modeling surface tension. J Comput Phys 1992;100:335–54.
[24] Muzaferija S, Peric M, Sames P, Schellin T. A two-fluid Navier–Stokes solver to simulate water entry; 1998.
[25] Ubbink O, Issa RI. A method for capturing sharp fluid interfaces on arbitrary meshes. J Comput Phys 1999;153:26–50.
[26] Youngs DL. Time-dependent multi-material flow with large fluid distortion. Numer Methods Fluid Dynam 1982;24:273–85.
[27] Issa R. Solution of the implicitly discretised fluid flow equations by operator-splitting. J Comput Phys 1985;62:40–65.
[28] Renardy Y, Renardy M. PROST: a parabolic reconstruction of surface tension for the volume-of-fluid method. J Comput Phys 2002;183(2):400–21.
[29] Francois MM, Cummins SJ, Dendy ED, Kothe DB, Sicilian JM, Williams MW. A balanced-force algorithm for continuous and sharp interfacial surface tension models within a volume tracking framework. J Comput Phys 2006;213(1):141–73.
[30] Harvie DJ, Davidson MR, Rudman M. An analysis of parasitic current generation in Volume of Fluid simulations. Appl Math Model 2006;30:1056–66.
[31] Lafaurie B, Nardone C, Scardovelli R, Zaleski S, Zanetti G. Modelling merging and fragmentation in multiphase flows with SURFER. J Comput Phys 1994;113(1):134–47.
[32] Horgue P, Augier F, Quintard M, Prat M. A suitable parametrization to simulate slug flows with the Volume-Of-Fluid method. CR Mec 2012;340(6):411–9.
[33] Popinet S. An accurate adaptive solver for surface-tension-driven interfacial flows. J Comput Phys 2009;228(16):5838–66.
[34] Pianet G, Vincent S, Leboi J, Caltagirone J, Anderhuber M. Simulating compressible gas bubbles with a smooth volume tracking 1-fluid method. Int J Multiph Flow 2010;36(4):273–83.
[35] Dupont J-B, Legendre D. Numerical simulation of static and sliding drop with contact angle hysteresis. J Comput Phys 2010;229(7):2453–78.
[36] Huang H, Meakin P, Liu M. Computer simulation of two-phase immiscible fluid motion in unsaturated complex fractures using a volume of fluid method. Water Resour Res 2005;41(12).
[37] Yarin AL. Drop impact dynamics: splashing, spreading, receding, bouncing, etc.. Annu Rev Fluid Mech 2006;38(1):159–92.
[38] Fujimoto H, Shiotani Y, Tong AY, Hama T, Takuda H. Three-dimensional numerical analysis of the deformation behavior of droplets impinging onto a solid substrate. Int J Multiph Flow 2007;33(3):317–32.
[39] Wang M-J, Lin F-H, Ong JY, Lin S-Y. Dynamic behaviors of droplet impact and spreading – water on glass and paraffin. Colloids Surfaces A Physicochem Eng Asp 2009;339(1–3):224–31.